

COMPARISON OF MODELS FOR THE SIMULATION OF FATIGUE-DRIVEN DELAMINATION USING COHESIVE ELEMENTS

K. Kiefer^{*}, P. Robinson & S.T. Pinho

Department of Aeronautics, Imperial College London, UK

* Corresponding author(K.kiefer09@imperial.ac.uk)

Keywords: *delamination, high-cycle fatigue, cohesive elements, numerical modeling*

Abstract

In this paper, two formulations for introducing fatigue damage into cohesive elements have been examined to determine their mesh sensitivity and numerical stability in mode I. A simple, non-FE model has been used to quickly assess a wide range of parameters associated with the fatigue degradation routines developed for cohesive elements. The model has been used to explore the sensitivity of two fatigue degradation strategies to changes in key parameters. For small element and cycle increments, both models predict the fatigue crack growth rate accurately for various applied loads where the Paris law is valid. However the models exhibit significant mesh sensitivities. The analysis has shown that in order to obtain a numerically stable algorithm, the models need to be improved.

1 Introduction

Laminated carbon fibre reinforced polymer composites can fail in a variety of modes. One key failure mode is delamination, in which the layers in the laminate separate. This can result in a considerable loss of structural stiffness and strength. Delaminations occur at locations in a structure where interlaminar stresses are high, for example at free edges, ply drops and corners. These stresses can be caused by static loads as well as dynamic ones (such as impact) but the case of interest here is delamination due to cyclic loading. A particularly concerning aspect of delamination is that it often develops without any readily visible external sign and requires the use of non-destructive testing methods (such as ultrasound-based techniques) to establish the full extent of the damage. It is therefore of considerable interest to be able to model

delamination numerically so as to understand how delaminations might develop in a particular structural design and how the design could be improved to be less susceptible to delamination. One way of doing this in finite element (FE) models is through the use of cohesive (or interface) elements [1], which have been used extensively for delamination growth under quasi-static loading. More recently cohesive elements have been adapted to also model fatigue-driven delamination [2,4]. In this paper, two of these formulations for introducing fatigue damage into cohesive elements have been examined to determine their mesh sensitivity and numerical stability in mode I.

2 Cylinder Model

For the investigations undertaken here, Finite Element Analyses are relatively time-consuming. Therefore, a mathematical non-FE model was used which was previously developed to enable a more rapid assessment of potential fatigue modeling strategies [3].

This model, referred to as the cylinder model, consists of two zero-thickness layers of width W . The bottom layer is attached to the ground and the top one to a cylinder of sufficiently large radius R (see Figure 1). The interface response between the layers is modelled through initially unstressed vertical springs with an equidistant spacing Δl with the first spring at $x=0$. The role of the springs in this model is to replicate the behaviour of the cohesive elements in the FE implementation. The springs can be associated with a constitutive law and a damage model to account for static and fatigue loading. The springs are assumed to remain vertical as the cylinder rotates. When a constant clockwise moment $M_a < M_c$ is applied to the cylinder, it rotates and the point of contact moves from $x=0$ initially to a new equilibrium position x_c where the resistance of the springs is equal to the applied moment. M_c is the

critical moment at which the springs fail statically, so no equilibrium position can be found anymore. Applying a moment equal to or greater than M_c leads to static crack propagation. When the cylinder is in equilibrium, the externally applied moment M_a must be equal and opposite to the moment M_t applied by the springs, which are resisting the rotation of the cylinder, about the contact point. In case the rotation θ or contact point x_c is known, this moment can be calculated in a straightforward way by first calculating the spring extensions and from those the spring traction. From the tractions, a spring force can be calculated and from the forces the moment exerted by each spring. Summing up the moment over all the springs about the contact point then gives the total moment M_t . The x -coordinate of the contact point x_c of the cylinder for a certain angle θ is $x_c = \theta R$. The number of active springs N_s in the interface is then

$$N_s = \left\lfloor \frac{\theta R}{\Delta l} \right\rfloor + 1, \quad (1)$$

where $\lfloor x \rfloor$ denotes the largest integer smaller than x . The springs are numbered from 1 to N_s beginning with the spring at the origin; x_i is the x -coordinate of the i th spring (see Figure 2). The extension δ_i of the i th spring then is

$$\delta_i = R - R \cos(\sin^{-1} \frac{x_c - x_i}{R}). \quad (2)$$

The traction-separation response $\sigma(\delta)$ is expressed through a static constitutive law (see Figure 3). For the fatigue degradation algorithms implemented in this paper, the bilinear law was used, which is shown in Figure 3 and is described analytically as

$$\sigma(\delta) = \begin{cases} K\delta & \text{for } 0 \leq \delta \leq \delta_0 \\ \sigma_0 \left(\frac{\delta_c - \delta}{\delta_c - \delta_0} \right) & \text{for } \delta_0 < \delta \leq \delta_c, \\ 0 & \text{for } \delta_c < \delta \end{cases} \quad (3)$$

where $K = \sigma_0 / \delta_0$. The parameters for the cylinder as well as the bilinear law are given in Table 1 and are chosen, so that the area under the cohesive law is equal to G_c .

Table 1 Cylinder and constitutive law properties

Cylinder	$R=100\text{mm}$	$W=1\text{mm}$
Constitutive law	$\sigma_0 = 30 \text{ N/mm}^2$	$\delta_0 = 1.e-6\text{mm}$
	$G_c = 0.26 \text{ N/mm}$	$\delta_c = 0.0173\text{mm}$

In the static case, the spring force can be calculated as the product of the area that is represented by the spring ($\Delta l W$) and the traction $\sigma_i(\delta_i)$. An exception is the first spring where the represented area is $\frac{1}{2} W \Delta l$. The total moment that is exerted by the springs is

$$M_t = \frac{1}{2} \sigma_1 \cdot \Delta l \cdot W \cdot x_c + \sum_{i=2}^{N_s} \sigma_i \cdot \Delta l \cdot W (x_c - x_i) \quad (4)$$

If an external moment M_a is applied, the equilibrium position of the cylinder is unknown and has to be approximated through iteration algorithm. In the fatigue models discussed here, the load is applied in two steps. Firstly a static moment M_a is applied to the cylinder and the equilibrium position x_c is found. Since the aim is to model high-cycle-fatigue, it is too computationally expensive to model every loading cycle. The numerically applied load in the second step is therefore kept at the constant level M_a throughout the algorithm until the final number of cycles N_{max} has been reached.

The degradation of the interface elements is controlled by a damage variable D , which is a function of the displacement of the spring as well as the number of cycles, for each element. In the fatigue degradation, the remaining traction σ is computed as a function of the damage and the displacement $\sigma(\delta, D)$. In order for the models to be computationally feasible, in each step a number of cycles ΔN are processed and the displacements are taken as the maximum values.

3 Models

3.1 Peerlings model

This model was originally developed by Robinson et al. [2]. The static constitutive relationship used is the bilinear law mentioned in equation (3). The traction with respect to the damage is expressed as follows

$$\sigma = (1 - D) K \delta, \quad (5)$$

where the damage is divided into a static and a fatigue part, D_s and D_f respectively for which $D = D_s + D_f$. The static damage can be written in terms of the displacement using equations (3) and (5) as

$$D_s(\delta) = \begin{cases} 0 & \text{for } 0 \leq \delta \leq \delta_0 \\ \frac{\delta_c - \delta}{\delta_c - \delta_0} & \text{for } \delta_0 < \delta \leq \delta_c \\ 1 & \text{for } \delta_c < \delta \end{cases} \quad (6)$$

The change in static damage between N cycles and $N + \Delta N$ can then be computed from the respective displacements and equation (6) as

$$\Delta D_s = \frac{\delta_0 \delta_c}{\delta_c - \delta_0} \left(\frac{1}{\delta(N)} - \frac{1}{\delta(N + \Delta N)} \right). \quad (7)$$

The fatigue damage is introduced in the following way which was originally proposed by Peerlings [5]

$$\dot{D}_f = \frac{\partial D_f}{\partial t} = C e^{\lambda D} \left(\frac{\delta}{\delta_a} \right)^\beta \frac{\dot{\delta}(t)}{\delta_a} \quad (8)$$

where β , λ , and C are parameters which have to be determined so that the resulting crack growth is in agreement with the experimentally determined Paris law and δ/δ_a is a normalized displacement. The constants used in this study are shown in Table 2.

Table 2 Peerlings model [2] constants

$\beta=2$	$\lambda=0.5$	$C=2.e-6$
-----------	---------------	-----------

Using this damage rate, fatigue damage can increase also, when the initial damage is zero and thus a crack can grow even in an initially undamaged interface. The derivation of the damage growth rate per cycle is explained in detail in [2], is given by:

$$\frac{\partial D_f}{\partial N} = \frac{C}{1 + \beta} e^{\lambda D} \left(\frac{\delta}{\delta_c} \right)^{1+\beta}. \quad (9)$$

The fatigue damage after a number of cycles ΔN has elapsed can then be found by integrating equation (9) over the respective number of cycles. This integration is performed numerically. A constant μ , $0 \leq \mu \leq 1$ is found, so that

$$\Delta D_f = \int_N^{N+\Delta N} \frac{\partial D_f}{\partial N} dN = \Delta N \frac{\partial D_f(D_\mu, \delta_\mu)}{\partial N}, \quad (10)$$

$$\begin{aligned} D_\mu &= (1 - \mu)D(N) + \mu D(N + \Delta N) \\ \delta_\mu &= (1 - \mu)\delta(N) + \mu\delta(N + \Delta N). \end{aligned} \quad (11)$$

In this paper, a value for μ of 0.7 was used. Combining equations (7) and (10), the damage evolution with respect to a cycle jump ΔN can thus be expressed as

$$D(N + \Delta N) = D(N) + \Delta D_s + \Delta D_f \quad (12)$$

This is an implicit formulation for $D(N + \Delta N)$ which is approximated using a Newton-Raphson algorithm.

Results

Figure 4 shows several x_c vs. N curve for an applied moment of 20% of M_c . The crack tip is located at $x = x_c - l_{cz}$, where l_{cz} is the length of the cohesive zone.

Once the curve has reached the steady state, the length of the cohesive zone is constant so that the crack growth rate $\frac{da}{dN} = \frac{dx_c}{dN}$ can be calculated as the slope of the linear part of the x_c vs. N curve. As the element size is increased, the x_c vs. N curve exhibits kinks. The tips of these kinks have a vertical separation of Δl and the crack growth rate $\frac{dx_c}{dN}$ is found by taking into account a crack growth Δx which is an integral number of element sizes.

The traction-separation relation including fatigue degradation is shown in Figure 5, where the areas under the curves represent G_a , the applied energy release rate. As the value for the applied moment M_a increases, the interface approaches the static constitutive law. Since the crack growth rate rises exponentially, there is a decreasing number of individual points on the graphs for constant ΔN . In order to obtain accurate results for high applied moments, ΔN has therefore to be decreased. In Figure 5 the values chosen for Δl and ΔN are rather small. However, in order for the fatigue degradation strategy to be efficient, it is desirable that the model produces good results for a larger mesh size and a bigger number of cycle jumps. The relative error of the crack growth rate -with respect to the Paris law- is shown for an applied moment M_a which is 20% of M_c in Figure 6. This figure shows the oscillations in the error as Δl increases and the linear growth of the error with respect to ΔN . The plot also shows some radial lines pointing towards the origin. These may be due to a numerical instability in the algorithm.

3.2 Turon model

This model has been developed by Turon et al. [4] and uses a static damage model which is based on a bilinear constitutive law (3). The static damage with respect to the displacement is the same as in equation (6). This damage is related to the ratio of the damaged area A_d and the element area A_e which corresponds to the ratio of the energy that has been consumed by the element and the fracture toughness (see Fig. 3) through

$$\frac{A_d}{A_e} = \frac{\xi}{G_c} = 1 - \frac{\delta}{\delta_0} (1 - D) \quad (13)$$

The damaged area ratio can be expressed as follows by combining (7) and (13)

$$\frac{A_d}{A_e} = \frac{D\delta_0}{\delta_c(1 - D) + D\delta_0}. \quad (14)$$

The cyclic damage growth rate can be written as

$$\frac{\partial D}{\partial N} = \frac{\partial D}{\partial A_d} \cdot \frac{\partial A_d}{\partial N}, \quad (15)$$

where $\frac{\partial A_d}{\partial N}$ is the growth rate of the damaged area. The first term $\frac{\partial D}{\partial A_d}$ is obtained from equation (14)

$$\frac{\partial D}{\partial A_d} = \frac{1}{A_e} \frac{(\delta_c(1-D) + D\delta_0)^2}{\delta_c\delta_0}. \quad (16)$$

After ΔN cycles the damaged area ahead of the crack tip increases by ΔA_d . It is assumed that the increase in actual crack area ΔA is equivalent to the increase in the amount of damaged area. This is in turn equal to the increase in damaged area summed across all elements in the cohesive zone which lies ahead of the crack. The crack growth rate can then be related to the damaged area growth rates as follows:

$$\frac{\partial A}{\partial N} = \sum_{e \in A_{CZ}} \frac{\partial A_d^e}{\partial N}, \quad (17)$$

where A_d^e is the damaged area of an element and A_{CZ} is the area of the cohesive zone. Introducing the arithmetic mean $\frac{\partial A_d}{\partial N}$ of the individual damaged area growth rates $\frac{\partial A_d^e}{\partial N}$ in the cohesive zone, equation (17) can be rewritten as

$$\frac{\partial A}{\partial N} = \sum_{e \in A_{CZ}} \frac{\partial A_d^e}{\partial N} = \frac{A_{CZ}}{A_e} \frac{\partial A_d}{\partial N} \Leftrightarrow \frac{\partial A_d}{\partial N} = \frac{A_e}{A_{CZ}} \frac{\partial A}{\partial N}.$$

Combining equations (15), (16), and (17), the overall damage rate is obtained

$$\frac{\partial D}{\partial N} = \frac{1}{A_{CZ}} \frac{(\delta_c(1-D) + D\delta_0)^2}{\delta_c\delta_0} \frac{\partial A}{\partial N}, \quad (18)$$

For A_{CZ} , the actual cohesive zone area from the cylinder model has been used in the present paper while the Turon et al. [4] cite Rice's closed form equation for pure mode I to calculate A_{CZ} [6]. The crack growth rate $\frac{\partial a}{\partial N}$ is assumed to evolve according to the Paris law

$$\frac{da}{dN} = C \left(\frac{G_a}{G_c} \right)^m, \quad (19)$$

where $G_{th} < G_a < G_c$, and $\frac{\partial a}{\partial N}$ is related to $\frac{\partial A}{\partial N}$ in equation (18) through $\frac{\partial A}{\partial N} = \frac{\partial a}{\partial N} W$. Here G_{th} is the threshold value for the energy release rate above which the Paris law can be applied and G_c is the

fracture toughness. The Paris law parameters C and m , and G_c are material constants that have to be determined experimentally. The constants used here are shown in Table 3.

Table 3 Turon model [4] constants

$C=0.0616$	$m=5.4$	$G_c=0.26 \text{ N/mm}$
------------	---------	-------------------------

G_a is the applied energy release rate which the authors compute from the constitutive law of the cohesive zone model

$$G_a = \int_0^\delta \sigma(\delta) d\delta. \quad (20)$$

The damage growth rate from equation (18) is then used to compute the damage of the elements in each step iteratively. The damage of the i th element in the j th step after increasing the number of cycles by ΔN can be found through the following equation

$$D_j^i = D_{N+\Delta N_j}^i = D_{j-1}^i + \frac{\partial D_{j-1}^i}{\partial N} \Delta N_j. \quad (21)$$

The number of cycles that are processed is calculated for each step as

$$\Delta N = \frac{\Delta D}{\max_i \left\{ \frac{\partial D^i}{\partial N} \right\}}, \quad (22)$$

where ΔD , which needs to be specified before running the algorithm, is the maximum allowable damage increment of one element across all elements in the cohesive zone. During every cycle jump the fatigue degradation is followed by an equilibrium step.

Results

There is no transition zone in the crack growth vs. cycles, but the crack grows linearly from the beginning of the fatigue cycling. There are also no kinks as the element size is increased. When the actual cohesive zone is used that develops in the cylinder model, the Paris law is underestimated. The best fit was obtained when this cohesive zone area was scaled by a factor of 0.3.

The traction-separation law including fatigue is shown in Figure 7. The sharp kinks in the graph result from the fact that the fatigue damage degradation is treated separately from finding the static equilibrium, with the vertical parts representing the drop in interface strength due to fatigue. The area under the curve extrapolated from

the equilibrium positions (the peaks in the graph) represents the applied energy release rate G_a . The number of cycles per step ΔN is variable and controlled by ΔD and in this case the chosen value is small enough to ensure a sufficient number of points on the traction-separation response for all values of the applied moment monitored. The sensitivity of the algorithm was examined with respect to the element size Δl and the maximum allowed damage ΔD .

The relative error was computed from the Paris law that served as a model input. The resulting error plot for an applied moment M_a of 20% of M_c is shown in Figure 8. The plot shows again some oscillation as the mesh size is increased but it is not as pronounced as in the previous algorithm and the bands where the error is similar are not parallel to the ΔD axis as they were to the ΔN -axis previously. However the errors are significantly higher than in the previous algorithm and the instabilities as the element size Δl and ΔD (see equation (22)) are increased are more chaotic.

4 Conclusions

Both models described in the previous section have been implemented in MATLAB and in FORTRAN 90. They are both sensitive to the mesh size and the step size controlled by ΔN (Peerlings model [2]) or ΔD (Turon model [4]) respectively. The models converge to the correct crack growth rate as these parameters are reduced. The model by Turon et al. [4] is computationally cheaper and there is no transition phase as in the model by Robinson et al. [2], but it shows larger and also more chaotic errors. The computational cost in the Robinson model could also be reduced by changing the implicit calculation of the damage rate per cycle $\frac{\partial D}{\partial N}$ to an explicit version.

5 Acknowledgements

This research has received funding from the European Community's Seventh Framework Program FP7/2007-2013 under grant agreement n°213371 (www.maaximus.eu).

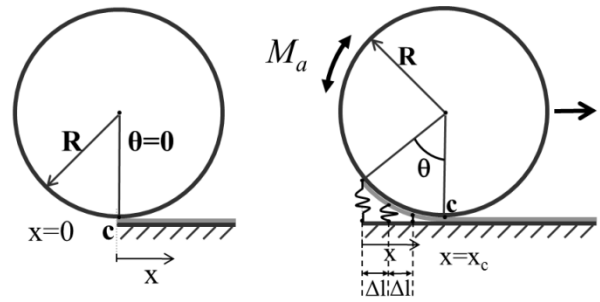


Figure 1 Cylinder model showing extended springs, element spacing Δl and contact point x_c

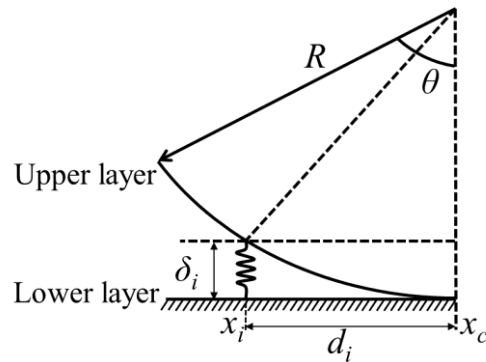


Figure 2 Schematic drawing of the i th spring

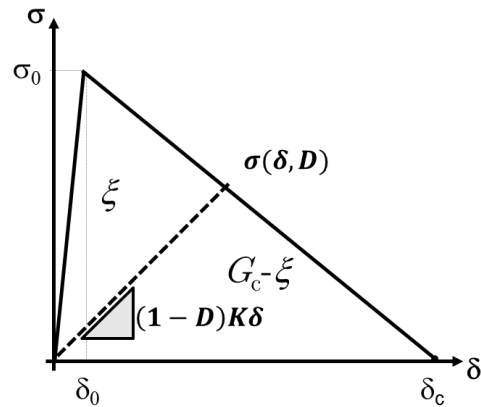


Figure 3: Bilinear cohesive law (see equation (3))

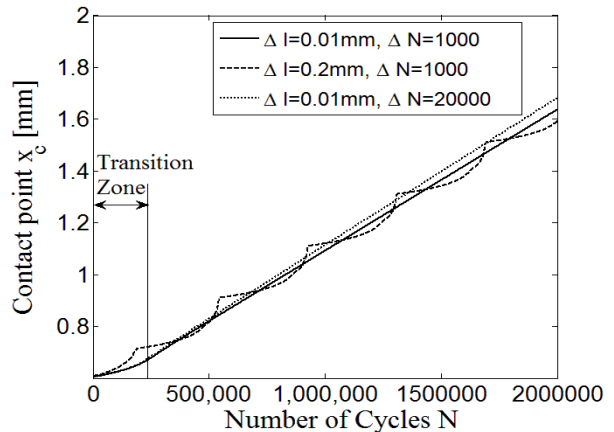


Figure 4 x_c vs. N curves for 20% M_c ,

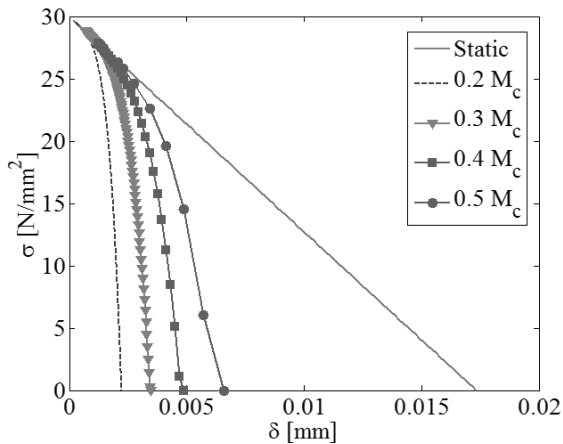


Figure 5 Peerlings model constitutive law including fatigue, $\Delta l=0.01\text{mm}$, $\Delta N=1000$ cycles

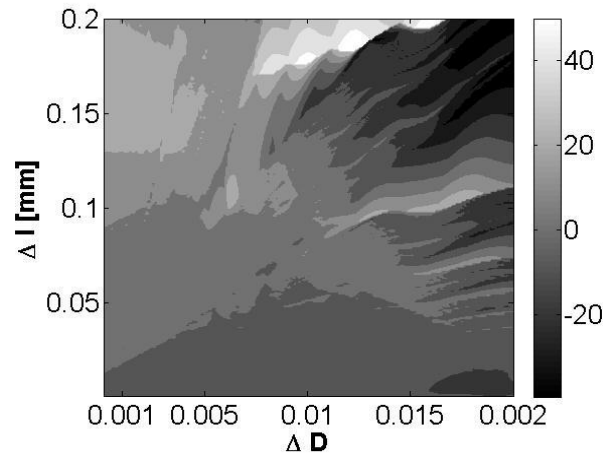


Figure 8 Sensitivity analysis of the model by Turon et.al. [4] at 20% of the static critical moment M_c

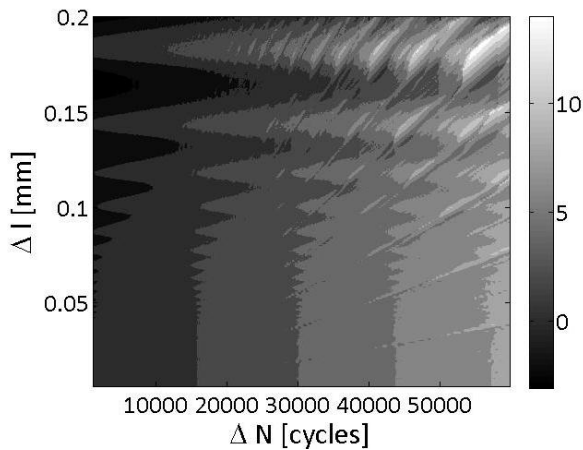


Figure 6 Sensitivity plot of the model by Robinson et.al [2] at 20% of the static critical moment M_c

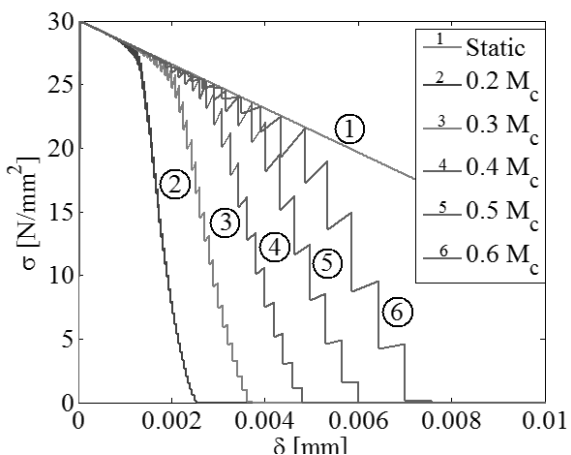


Figure 7 Turon model constitutive law including fatigue

- [1] JCJ Schellekens, R. de Borst “A non-linear finite element approach for the analysis of mode-I free edge delamination in composites”. *Int. J. Solids Structures* 30, 1239–1253, 1993
- [2] Robinson P, Galvanetto U, Tumino D, Bellucci G., and D.Violeau “Numerical simulation of fatigue-driven delamination using interface elements”. *Int J Numer Meth Eng* 2005;63:1824–48.
- [3] U. Galvanetto, P. Robinson, A. Cerioni; C. Lopez Armas “A Simple Model for the Evaluation of Constitutive Laws for the Computer Simulation of Fatigue-Driven Delamination in Composite Materials”. *SDHM: Structural Durability & Health Monitoring*, Vol. 5, No. 2, pp. 161-190, 2009
- [4] Turon, J. Costa, P.P. Camanho, and C.G. Davila “Simulation of delamination in composites under high-cycle fatigue”. *Composites Part A: Applied Science and Manufacturing*, Volume 38, Issue 11, November 2007, Pages 2270-2282
- [5] R.Peerlings, W.Brekelmans, R.de Borst, M.Beers “Gradient-enhanced damage modelling of high-cyclic fatigue”. *International Journal for Numerical Methods in Engineering*, Volume 49, 2000, pp 1457-1569
- [6] J. R. Rice “The mechanics of earthquake rupture”. *Physics of the Earth's Interior*, edited by A.M. Dziewonski and E. Boschi, Italian Physical Society/ North Holland Publ. Co., 1980, pp.555—649